Study of Cr/Sc-based multilayer reflecting mirrors using soft x-ray reflectivity and standing wave-enhanced x-ray fluorescence

Meiyi Wu, Catherine Burcklen, Jean-Michel André, Karine Le Guen, Angelo Giglia, Konstantin Koshmak, Stefano Nannarone, Françoise Bridou, Evgueni Meltchakov, Sébastien de Rossi, et al.

Study of Cr/Sc-based multilayer reflecting mirrors using soft x-ray reflectivity and standing wave enhanced x-ray fluorescence

Meiyi Wu[a,b], Catherine Burcklen[c], Jean-Michel André[a,b], Karine Le Guen[a,b], Angelo Giglia[d], Konstantin Koshmak[d], Stefano Nannarone[d], Françoise Bridou[c], Evgueni Meltchakov[c], Sébastien de Rossi[c], Franck Delmotte[c], Philippe Jonnard[a,b,*]

[a]Sorbonne Universités, UPMC UnivParis 06, Laboratoire de Chimie Physique - Matière et Rayonnement, 4 Place Jussieu, Paris, France, 75252
[b]CNRS UMR 7614, Laboratoire de Chimie Physique - Matière et Rayonnement, 4 Place Jussieu, Paris, France, 75252
[c]Institutd'Optique Graduate School, Laboratoire Charles Fabry, CNRS, Université Paris-Saclay, Palaiseau Cedex, France, 91127
[d]CNR, Istituto Officina Materiali, Strada Statale 14 km 163,5, Trieste, Italy, 34149

Abstract. We study Cr/Sc-based multilayer mirrors designed to work in the water window range using hard and soft x-ray reflectivity as well as x-ray fluorescence enhanced by standing waves. Samples differ by the elemental composition of the stack, the thickness of each layer and the order of deposition. This paper mainly consists of two parts. In the first part the optical performances of different Cr/Sc-based multilayers are reported, and in the second part we extend further the characterization of the structural parameters of the multilayers which can be extracted by comparing the experimental data with simulations. The methodology is detailed in the case of Cr/B_4C/Sc sample for which a three-layer model is used. The structural parameters determined by fitting reflectivity curve are then introduced as fixed parameters to plot the x-ray standing wave curve, to compare with the experiment and confirming the determined structure of the stack.

Keywords: Cr/Sc, multilayers, Bragg diffraction, soft x-ray reflectivity, x-ray fluorescence, x-ray standing waves.

***Philippe Jonnard, E-mail: philippe.jonnard@upmc.fr

1 Introduction

Periodic multilayer mirrors play an important role as optical components in the x-ray and extreme ultraviolet (EUV) spectral ranges for applications such as space telescopes, x-ray microscopes, EUV photolithography and optical components of beamlines in synchrotron radiation facilities. Such mirrors have high peak reflectivity at the wavelength of interest. A well-defined structure of the multilayer with fine details of each layer and each interface is crucial for

the development and improvement of the design work, which is why we dedicated our time and effort to characterize it.

The Cr/Sc multilayer system discussed in this paper is designed for the development of a high reflective mirror working in the water window range (2.3 – 4.4nm)[1]. Based on the Cr/Sc bilayer, derivative systems were also fabricated. Firstly B4C barrier layer was inserted to increase the thermal stability and to decrease the interdiffusion between Cr and Sc layers[2]. It has been reported that this kind of third material placed on interfaces of the original multilayer structure exhibits increased reflectivity in multiple systems such as Mo/Si[3,4], Sc/Si[5,6], Si/Gd[7] and Co/Mg[8]. Such material was inserted at either Cr-on-Sc or Sc-on-Cr interfaces and should lead to different optical performances following the model of Larruquert[9]. Secondly, a CrN/Sc sample was also fabricated by adding nitrogen into the sputtering gas (argon) during deposition; this would decrease the interdiffusion and sharpen the interfaces[10,11], and thus a higher reflectivity is expected.

In this paper a XRR study will be presented first. The optical performances of all studied multilayer mirrors at their application energy will be compared. It has been decades that scientists use softwares to create models to simulate and fit the x-ray reflectivity (XRR) data in order to determine the structure of multilayers[12]. We present the fitting of the soft XRR data to explore the structure (layer thickness and interface roughness) of the multilayers.

Second, we also use another method: standing wave enhanced x-ray fluorescence (XRF-XSW). Pioneered by B. W. Batterman in the 1960s[13], the x-ray standing wave (XSW) technique can be used to study the structure of surfaces and interfaces of multilayers made of nanoscale thin films with high depth resolution and chemical selectivity[14-17]. The interferences between the incident and the reflected beams generate a x-ray standing wave field where the amplitude on

anti-nodal plane is maximized and the amplitude on the nodal plane is minimized. Such feature is suitable for periodic multilayer study as it makes the experimental acquisition specific on certain interfaces located on the anti-nodal plan. When the reflected beam is generated at the Bragg condition for a super-lattice like the periodic Cr/Sc multilayer, the period of the XSW equals the periodicity of the reflecting planes. By scanning the fluorescence yield around the Bragg angle, the position of the elements on either side of the interface can be revealed.

2 Experimental details

Samples were prepared by using magnetron sputtering with no substrate bias. The purity of Cr, Sc and B4C targets was better than 99.9%. The substrates were sliced and polished Si (100) wafers. Pure Ar gas was used for Cr, Sc and B4C layers whereas a mixture of Ar and N2 gas (80% Ar, 20% N2) was used for CrNx deposition. The Cr and CrNx layers were deposited by DC magnetron sputtering with a 50 mA current. Sc and B4C layers were deposited by RF magnetron sputtering with a power of 50 and 150 W respectively. The thickness of each layer was determined by the velocity of the substrate over the deposition area. The original design was 100 periods of Cr/Sc bilayer covered by a 3 nm-thick B4C capping layer in order to protect the sample from oxidization. Hard XRR measurements were performed using a commercial grazing incident reflectometer (BRUKER Discover D8) equipped with Cu K radiation source (8048 eV). Table 1 presents for each sample the detailed structural parameters as designed and extracted from the fitting of the measured XRR curve. The notation of sample structure starts from the substrate. The measured period values are different from the expected values for the deposition. For example, samples 2 and 3 were both expected to have 2.2 nm for each period, yet the determined values are 1.72 nm. Such a change of the period (contraction) is due to the intermixing of different layers which will be described later.

Table 1. Structural parameters of the samples as designed and extracted from the fitting of the measured hard XRR curves.

Sample	Structure	Period (nm)	Cr (nm)	Sc (nm)	B_4C (nm)	Measured period (nm)
1	$[B_4C/Cr/Sc]_{100}$ + B_4C cap	1.9	0.6	1.0	0.3	1.65
2	$[Cr/B_4C/Sc]_{100}$ + B_4C cap	2.2	0.6	1.0	0.6	1.72
3	$[B_4C/Cr/Sc]_{100}$ + B_4C cap	2.2	0.6	1.0	0.6	1.72
4	$[B_4C/Cr/Sc]_{100}$ + B_4C cap	2.5	0.6	1.0	0.9	1.83
5	$[Cr/Sc]_{100}$ + B_4C cap	1.6	0.6	1.0	/	1.58
6	$[CrN/Sc]_{100}$ + B_4C cap	1.6	0.6(CrN)	1.0	/	1.66

Soft x-ray characterization was done using XRR and XRF-XSW. Experiments were performed on the BEAR beamline at the ELETTRA synchrotron radiation center[18]. The choice of the incident photon energy for XRR measurements was made in accordance with x-ray absorption spectroscopy (XAS) data measured in the total electron yield mode. The retained value is corresponding to the maximum of the first XAS peak associated to the Sc L3 and Cr L3 absorption edges. For XSW measurements we chose the energy associated to Cr L3 edge. The angle between the incident beam and the fluorescence detector, a silicon drift detector (SDD), was fixed at 60°. The fluorescence light was measured selecting the energy window around the Cr L emission (572.8 eV). Being that the energy resolution of the detector is about 100 eV, in this way we excluded the contribution coming from Sc L emission (395.4 eV). The intensity of Cr L emission was scanned as a function of the grazing incident angle, leading to the so-called XSW curve.

3 Result and discussions

Fig. 1 presents the XRR curves measured at the application photon energy equal to 395 eV. Fig. 1(a) displays the comparison of all samples. As expected from the values in Table 1, the

smallest value of the period gives rise to the highest of the Bragg angle. In addition the peak reflectivity and bandwidth differs from one sample to another. An obvious difference in reflectivity can be observed in Fig. 1(b) between sample 2 (namely Cr/B4C/Sc) and sample 3 (B4C/Cr/Sc) which only differ by the order of the layers. For sample 2, B4C barrier layers are located at Sc-on-Cr interfaces while for sample 3, they are located at Cr-on-Sc interfaces. The higher reflectance of sample 2 is in line with the prediction of the theoretical model of Larruquert[19] which considers the contrast of refractive index of the materials for a given deposition order in a single period. Such difference may also have other origin such as the difference in interdiffusion between B4C-on-Cr and B4C-on-Sc interfaces. Another group of comparisons is formed with samples 1, 3 and 4 (Fig. 1(c)) where the only changing parameter is the thickness of B4C layer varying from 0.3 nm to 0.9 nm. The Bragg peak is (as expected) shifted according to the period change while the reflectivity remains almost constant. The last comparison (Fig. (1d)) concerns the two bilayer systems: sample 5 (Cr/Sc) and sample 6 (CrN/Sc). The introduction of nitrogen results in a doubled reflectance, which is probably due to sharpened interfaces[11]. Furthermore, the shift of the Bragg angle peak position indicates an increase of the period upon nitridation (in agreement with Table 1).

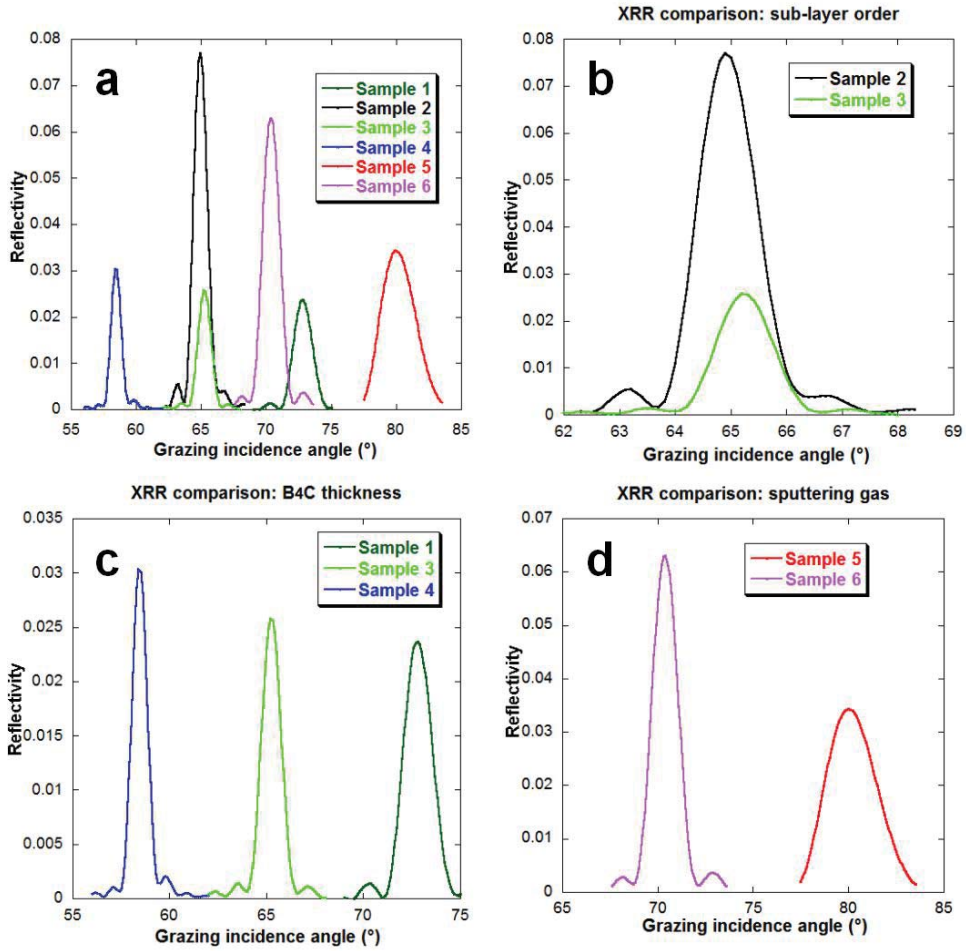

Fig. 1 XRR curves measured at 395 eV: (a) Overview for Cr/Scbased samples; (b) Comparison of the influence of layer order, samples 2 and 3; (c) Comparison of the influence of B_4C barrier layer thickness, samples 1, 3 and 4; and (d) Comparison of the influence of nitrogen in sputtering gas, samples 5 and 6.

Following the discussion of the optical performances of all samples, we illustrate the method how XRR and XRF data are used to get a reliable description of the stack by taking sample 2 (Cr/B4C/Sc tri-layer) as an example. According to the Ref. 20 the B4C layer is totally consumed by Cr: the barrier layer is actually a mixture which consist of 70% of Cr and 30% of B4C. We note the mixed barrier layer as CrB4C. The refractive index of the CrB4C used in the fitting process (carried out with IMD software[12]) is adjusted accordingly using the tabulated values of

Cr and B4C from CXRO database[21]. We consider a three layer model: the [Cr/CrB4C/Sc] structure repeats 100 times over Si substrate. A layer of B4C is put on top of such multilayer as capping layer.

We calculate the reflectivity while varying the parameters: thickness of each layer and roughness/interdiffusion of each interface. Fig. 2(a) and 2(b) show the XRR spectra of sample 2 measured with incident photon energy at 395 eV (application energy) and 574.8 eV (energy where we have the maximum absorption) respectively compared to the simulations. Between these two fittings, a variation of 1.4% for thickness and roughness of each layer is used. We believe such variation is tolerable as the experimental conditions may change slightly between the two individual experiments. For example the two XRR measurements were performed at different grazing incident angle range. This will cause a difference in the area of the illuminated area. Finally we obtained the following structure for sample 2: Cr(0.60 nm)/CrB_4C(0.20 nm)/Sc(0.92 nm), which is also compatible to the fitting of XRR measurement at 8048 eV. Such result shows a non-proportional deviation of the thicknesses for the different layers compared to the designed (expected) values. The severe intermixing also explains the tremendous change between aimed and measured thickness of each period shown in Table 1.

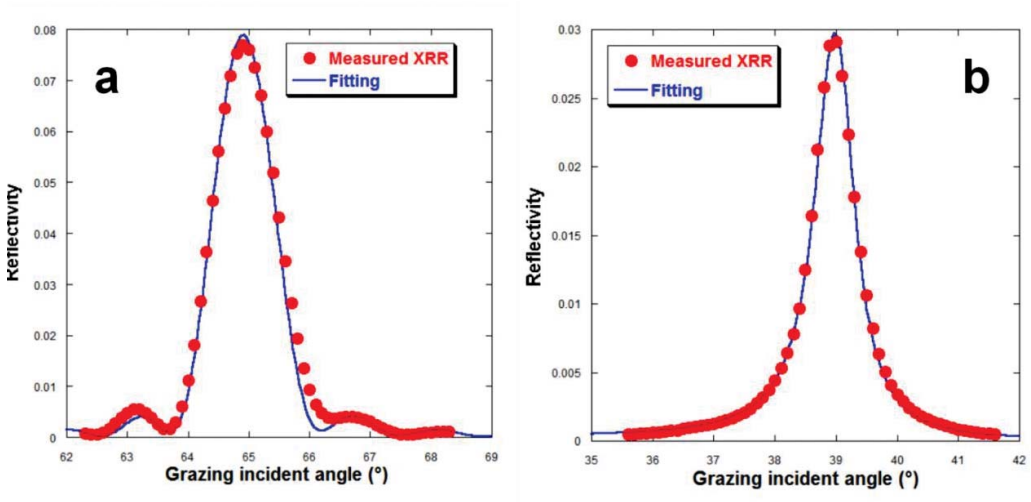

Fig. 2 XRR of sample 2 Cr/CrB_4C/Sc multilayer mirror at 395 eV(a) and 574.8 eV (b). Red dots: experiment; blue line: fit.

We use XRF-XSW to verify the structure we obtained from XRR fitting. The experimental result of XRF-XSW is compared with the simulation, which is done with the code FLUORT[22]. In the fluorescence calculation all parameters (thicknesses of the layers and roughness of each interface) determined from XRR fitting are applied. As shown in Fig. 3(a), for sample 2 (Cr/CrB_4C/Sc) the experimental XSW curve (red dots) is in agreement with the simulated curve (blue line) in terms of position, shape and amplitude of the intensity modulation. However, we could simulate experimental XRF data not only considering fluorescence emission but also taking into account diffuse scattering and Kossel effect in order to improve the determnation of the background in the angular range of interest. This is illustrated in Fig. 3(b) in the case of sample 3 (namely B_4C/Cr/Sc) on the 40 - 95° angular range. On the large-scale XSW curve, a first feature is located at 60° while a second structure is present around 80°. Such phenomenon happens to each sample with a varying intensity (the scattered intensity for sample 2 is low enough to be negligible). These features can be explained geometrically, taking into account that the angle between the incident x-ray beam and the SDD detector is fixed at 60°, as presented in Figure 4. The 60° grazing incident angle corresponds to the specular condition (see Fig. 4(a)) and the large tails on both sides of the peak is due to diffuse scattering. The scattered photons of the incident beam contribute to the background since the energy of the fluorescence photon (572.8 eV) is close to the one of the incident photon (575.2 eV) and cannot be resolved by the SDD detector. The secondary peak around 80° is due to the Kossel effect (see Fig. 4(b)), *i.e.* the diffraction of the radiation emitted by the periodic structure of the multilayer. Considering the large solid angle of detection in our experimental condition, such effect undergoes a convolution to form a wide and smooth peak. To take into account these two contributions (diffuse scattering

and Kossel diffraction), two Gaussian curves have been added to the original simulation of the XSW curve roughly centered at 60 and 80° respectively. In this way we obtain a better agreement in the zone of interest where standing wave feature takes place (Fig. 3(c)).

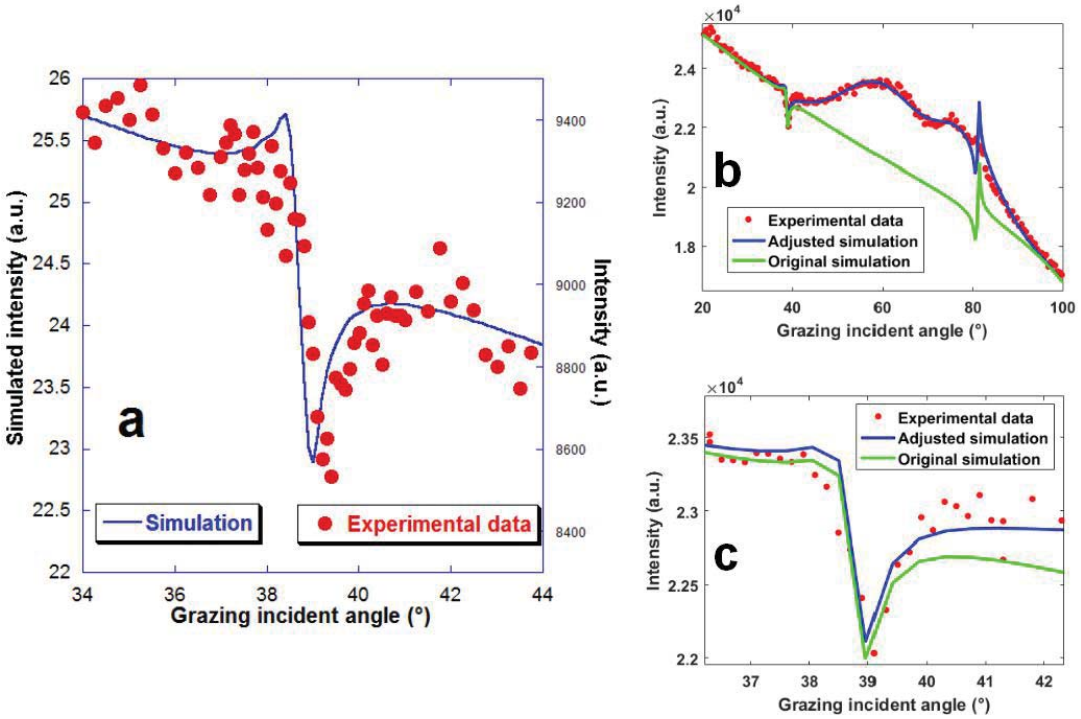

Fig 3 (a) XSW curve of the intensity of the Cr Lα emission of sample 2 Cr/B_4C/Sc multilayer mirror with an incident photon energy at 574.8 eV. (b) Large-scale angular scan of XSW curve at 575.2eV of sample 3 B_4C/Cr/Sc multilayer; red dots : experimental data; green line: raw simulation; blue line : simulation taking into account the diffuse scattering and Kossel effect. (c) Comparison of experimental curve and adjusted simulations for sample 3 in the zone of interest.

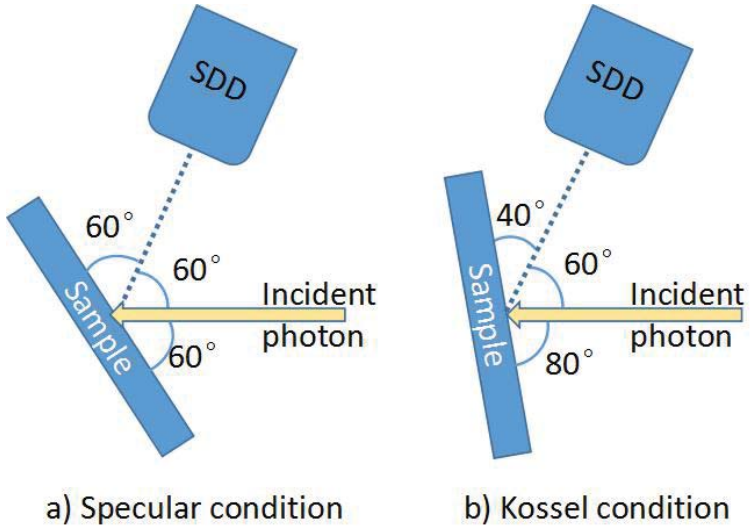

Fig. 4 XRF-XSW experimental geometry: there is a fixed angle of 60° between the directions of the incident and the detection of the emitted photons. The XSW curve is obtained by rotating the sample. (a) when the glancing angle of the photon beam on the sample surface is equal to 60°, the detector is in the specular direction; (b) when the glancing angle of the photons is around 80°, the Kossel condition is fulfilled because the detection angle corresponds to the value of the Bragg angle of the emitted radiation.

4 Conclusion and perspectives

We tested the performance of a series of multilayer mirrors based on the Cr/Sc system. B4C barrier layers are found to be more effective at Sc-on-Cr interfaces than at Cr-on-Sc interfaces to improve the reflectivity of the mirror. There is evidence that the introduction of nitrogen in the sputtering gas has positive effect for the improvement of the reflectivity of Cr/Sc system.

Two different methods, XRR and XRF-XSW, are simultaneously applied for the characterization of the Cr/CrB4C/Sc sample. In such way the determined structure of the sample is more reliable. To get a better fit of the XSW curve, we use an empirical model of the background originating from scattering and Kossel diffraction. Yet a mathematical calculation of the scattering is still in need to simulate it. For the moment the XRF-XSW simulation can be applied only as a verification method. But recent research declares success in fitting both XRR

and XRF curves together[23], and we are trying to develop our own fitting process to make it possible to determine the structure independently with XRF-XSW.

References

1. F. Schäfers et al., "Cr/Sc multilayers for the soft-x-ray range," *Appl. Opt.* **37** 719 (1998) [doi:10.1364/AO.37.000719].

2. M. Prasciolu et al., "Thermal stability studies of short period Sc/Cr and Sc/B_4C/Cr multilayers," *Appl. Opt.* **53**(10), 2126 (2014) [doi:10.1364/AO.53.002126].

3. S. Bajt et al., "Improved reflectance and stability of Mo-Si multilayers," *Opt. Eng.* **41**(8), 1797 (2002) [doi: 10.1117/1.1489426].

4. S. Braun et al., *Proc. SPIE* **5037** 274 (2003) [doi:10.1117/12.484984].

5. A. F. Jankowski et al., "Boron–carbide barrier layers in scandium–silicon multilayers," *Thin Solid Films* **469**–**470**, 372–376 (2004) [doi:10.1016/j.tsf.2004.08.153].

6. P. Jonnard et al., "Effect of B4C diffusion barriers on the thermal stability of Sc/Si periodic multilayers," *Surf. Sci.* **604**(11–12), 1015–1021 (2010) [doi:10.1016/j.susc.2010.03.012].

7. B. Kjornrattanawanich et al., "Normal-incidence silicon–gadolinium multilayers for imaging at 63 nm wavelength" *Opt. Lett.* **33** 965 (2008) [doi:10.1364/OL.33.000965].

8. K. Le Guen et al., "Introduction of Zr in nanometric periodic Mg/Co multilayers," *Appl. Phy. A* **102**(1), 69–77 (2011) [doi:10.1007/s00339-010-6093-2].

9. J. I. Larruquert, "Reflectance optimization of inhomogeneous coatings with continuous variation of the complex refractive index," *JOSA A* **23**(1), 99–107 (2006) [doi:10.1364/JOSAA.23.000099].

10. F. Eriksson et al., "Reflectivity and structural evolution of Cr/Sc and nitrogen containing Cr/Sc multilayers during thermal annealing," *J. Appl. Phys.* **104**(6), 063516 (2008) [doi:10.1063/1.2980051].

11. D. Xu et al., "Enhancement of soft X-ray reflectivity and interface stability in nitridated Pd/Y multilayer mirrors," *Opt. Express.* **23**(26), 33018 (2015) [doi:10.1364/OE.23.033018].

12. D. L. Windt, "IMD—Software for modeling the optical properties of multilayer films," *Comput. Phys.* **12**(4), 360 (1998) [doi:10.1063/1.168689].

13. B. W. Batterman et al., *Rev. Mod. Phys.* **36** 681 (1964). [doi:10.1103/RevModPhys.36.681a].

14. J. Zegenhagen, A. Kazimirov. *The X-Ray Standing Wave Technique: Principles and Applications* World Scientific (2013) [doi:10.1142/6666].

15. J. Zegenhagen, "Surface structure determination with X-ray standing waves," *Surf. Sci. Rep.* **18**(7–8), 202–271 (1993) [doi:10.1016/0167-5729(93)90025-K].

16. D. P. Woodruff, "Surface structure determination using x-ray standing waves," *Rep. Prog. Phys.* **68**(4), 743–798 (2005) [doi:10.1088/0034-4885/68/4/R01].

17. Y.-C. Tu et al., "X-ray fluorescence induced by standing waves in the grazing-incidence and grazing-exit modes: study of the Mg–Co–Zr system," *J. Sync. Rad.* **22**(6), 1419–1425 (2015) [doi:10.1107/S1600577515016239].

18. S. Nannarone, "The BEAR Beamline at Elettra," *AIP* **705** 450–453 (2004) [doi:10.1063/1.1757831].

19. J. I. Larruquert, "New layer-by-layer multilayer design method," *JOSA A* **19**(2), 385–390 (2002) [doi:10.1364/JOSAA.19.000385].

20. C. Burcklen et al., "Cr/B4C multilayer mirrors: Study of interfaces and X-ray reflectance," *J. Appl. Phys.* **119**(12), 125307 (2016) [doi:10.1063/1.4944723].

21. "CXRO X-Ray Interactions With Matter". http://www.cxro.lbl.gov/

22. J.-P. Chauvineau and F. Bridou, "Analyse angulaire de la fluorescence du fer dans une multicouche périodique Fe/C," Le Journal de Physique IV **6**(C7), C7–53 (1996) [doi:10.1051/jp4:1996707].

23. A. Haase et al., "Multiparameter characterization of subnanometre Cr/Sc multilayers based on complementary measurements," *J. Appl. Cryst.* **49**(6), 2161–2171 (2016) [doi:10.1107/S1600576716015776].

Caption List

Fig. 1 XRR curves measured at 395 eV: (a) Overview for Cr/Scbased samples; (b) Comparison of the influence of layer order, samples 2 and 3; (c) Comparison of the influence of B_4C barrier layer thickness, samples 1, 3 and 4; and (d) Comparison of the influence of nitrogen in sputtering gas, samples 5 and 6.

Fig. 2 XRR of sample 2 Cr/CrB4C/Sc multilayer mirror at 395 eV(a) and 574.8 eV (b). Red dots: experiment; blue line: fit.

Fig 3 (a) XSW curve of the intensity of the Cr Lα emission of sample 2 Cr/B4C/Sc multilayer mirror with an incident photon energy at 574.8 eV. (b) Large-scale angular scan of XSW curve at 575.2eV of sample 3 B4C/Cr/Sc multilayer; red dots : experimental data; green line: raw simulation; blue line : simulation taking into account the diffuse scattering and Kossel effect. (c) Comparison of experimental curve and adjusted simulations for sample 3 in the zone of interest.

Fig. 4 XRF-XSW experimental geometry: there is a fixed angle of 60° between the directions of the incident and the detection of the emitted photons. The XSW curve is obtained by rotating the sample. (a) when the glancing angle of the photon beam on the sample surface is equal to 60°, the detector is in the specular direction; (b) when the glancing angle of the photons is around 80°, the Kossel condition is fulfilled because the detection angle corresponds to the value of the Bragg angle of the emitted radiation.